Solid-State Battery Systems and Thermal Management for Electric Long-Distance Buses

Jan Friedrich Hellmuth¹ Markus Pollak² Andreas Schulte¹ Wilhelm Tegethoff¹ Jürgen Köhler¹

¹Institut für Thermodynamik, Technische Universität Braunschweig, Germany jan.hellmuth@tu-braunschweig.de

²TLK-Thermo GmbH, Braunschweig, Germany, m.pollak@tlk-thermo.com

Abstract

Solid-state batteries are promising for electric mobility as they potentially offer higher energy densities and therefore increased driving range, longer life and safety. They have different thermal properties and thermal management requirements than liquid battery systems. This paper presents a comparison of a solid-state battery system with a state-of-the-art liquid (Nickel-Manganese-Cobalt) NMC battery system for a simulated electric long-distance bus on a typical real-world long-distance route, requiring fast-charging. The battery characteristics are based on published data. Thermal management is performed by a reversible R744 heat pump. By designing both battery systems for the same energy capacity, the solid-state battery releases more heat during fast charging. For the same battery system size, the solid-state battery significantly outperforms the liquid battery system in driving range and does not require more cooling.

Keywords: Solid-State Battery, Thermal Management, Electric Mobility

1 Introduction

Electric mobility is on the rise worldwide and is recognized as a means to combat global warming and reduces local pollutant emissions (Sanguesa et al. 2021). Long-distance buses, also called coaches, are the most efficient transport option in terms of CO₂ emissions per person and kilometer (Thomas and Serrenho 2024; UK Department for Business Energy & Industrial Strategy 2022). In the current literature, solid-state batteries are discussed as the most promising alternative to state-ofthe-art lithium-ion batteries because they have higher energy densities (thereby increasing driving range) and better safety (Schmaltz, Hartmann, et al. 2023). Solid-state batteries come with different electrical and thermal characteristics (Yang et al. 2024) than lithium-ion batteries and offer a larger operating temperature range, extending operation to higher temperatures in particular (Schmaltz, Wicke, et al. 2022). The main difference is the higher internal electrical resistance compared to a liquid battery operating at the same temperature level (Janek and Zeier 2023). First evaluations for the thermal management of solid-state battery vehicles investigated cold start procedures (Hughes and Vagg 2022) and heat pumps for battery pre-heating (Hellmuth, Pollak, T. Heinke, et al. 2023). Kan et al. (2024) reviewed the thermal effects of solid-state batteries and discussed the higher amount of heat generation and the higher operating temperatures of solid-state batteries. Yang et al. (2024) compared the thermal and electrical characteristics of conventional liquid, semi-solid-state and Lithium-Iron-Phosphate (LFP) batteries based on experimental data. Ma et al. (2025) experimentally investigated solid-state batteries and modeled thermal and electrical characteristics. Li et al. (2025) compared semi-solid-state and liquid batteries.

In this study, the effects of solid-state battery implementation in a coach for long-distance operation are evaluated using system simulation in Modelica. The battery data of Yang et al. (2024) are implemented. The following contributions are provided:

- Comparison of state-of-the-art and solid-state batteries in the context of a long-distance bus
- Battery system sizing comparison
- Evaluation of thermal effects in a real-world driving scenario
- · Recommendations for the thermal management

2 Description of a coach model with solid-state batteries

To investigate the usage of solid-state batteries in a coach, we use a modular multi-scale vehicle model developed using Modelica (Modelica Association 2025) and integrated models from the TIL suite (TLK-Thermo GmbH 2024b). This approach allows for detailed simulation of electrical, mechanical and thermal interactions across various vehicle components. Similar modeling frameworks have been successfully applied to fuel-cell electric cars (S. Heinke et al. 2019) and to optimize thermal management systems in battery-electric trucks (Hellmuth, Steeb, Pollak, et al. 2023) as well as battery-electric coaches (Hellmuth, Pollak, Schulte, et al. 2024).

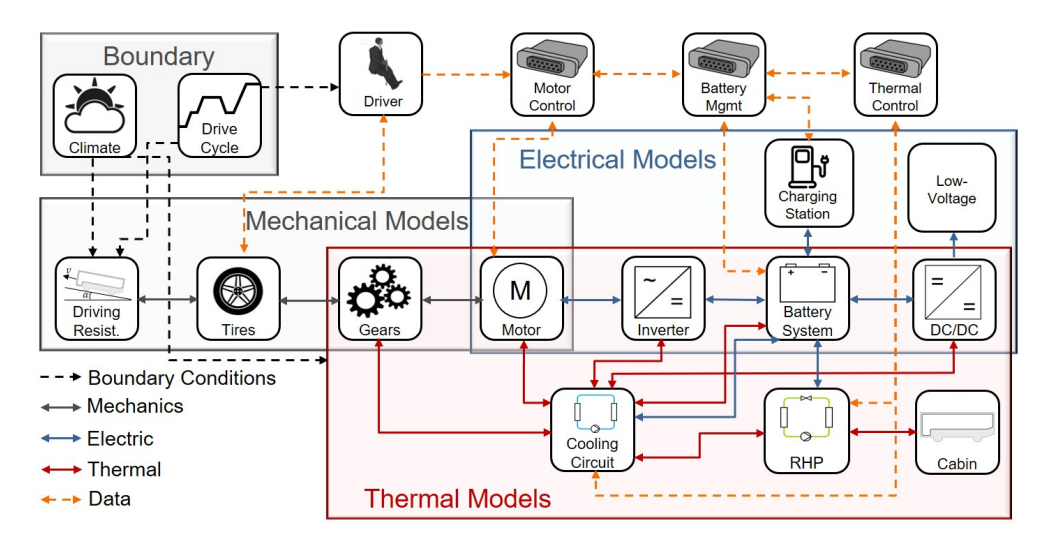


Figure 1. Model of an electric coach including balance rooms for flow variables (heat, electrical and mechanical power), control units, and data connections as well as boundary conditions and a charging station, adapted from Hellmuth, Pollak, Schulte, et al. (2024).

The comprehensive vehicle model is illustrated in Figure 1, highlighting key interactions and dependencies within the system. The balance rooms for the flow variables (heat, electrical, and mechanical power) as well as control units, data connections, and boundary conditions are visualized. The boundary conditions, thoroughly detailed in Section 3, encompass both climate data and a driving cycle. Specifically, we have defined ambient temperature, ambient humidity, and solar radiation as the primary climatic parameters. These factors not only affect driving resistance but also serve as boundary conditions for all thermal models. They have a significant impact on the cabin environment, the cooling circuit, and the reversible heat pump (RHP).

The drive cycle provides time-dependent data on the vehicle's speed and slope of the terrain. For the drive cycle we converted distance-based data into a time-based format. This fits well into the overall solution process of the formulated system of equations. A drive cycle from Karlsruhe to Munich is used in this study. This drive cycle was first described by Hebeler (2024) to investigate the potential of planetary gearboxes for the integration of a Rankine process in a coach. The drive cycle is displayed in Figure 2 showing the velocity and altitude along the route.

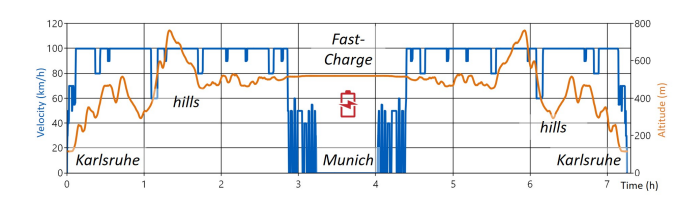


Figure 2. Drive Cycle showing the velocity and altitude profile for a long-distance coach trip from Karlsruhe to Munich and back and a fast-charging break, adapted from Hebeler (2024).

2.1 Mechanical Models for Drive-Train and Force

The mechanical subsystem includes models for driving resistance, tires, gears, and an electric motor to describe the driving dynamics of a configured vehicle. The driving resistance model, in particular, uses interchangeable parameter sets that include the drag coefficient c_w , frontal area A_{front} , vehicle weight $m_{vehicle}$, and rolling friction coefficient μ_{roll} . The parameters (Table 1) are taken from the $vanHool\ CX45E$ (Sustainable Bus 2020). Traction force is calculated by summing the four resistances:

$$F_{Traction} = F_{Roll} + F_{Air} + F_{Grade} + F_{Acceleration}$$
 (1)

Further description of the mechanical models can be found in (Hellmuth, Steeb, Pollak, et al. 2023; Hellmuth, Pollak, Schulte, et al. 2024).

Table 1. Vehicle parameters used in all scenarios.

Parameter	Value
Vehicle total mass	24 t
Frontal area	$7.5 m^2$
Drag coefficient	0.4
Rolling friction coefficient	0.006

2.2 Models of Electrical Components

The electrical motor model connects the mechanical and electrical models. Electrical power is calculated based on the required mechanical power. We assume a fixed motor efficiency of 95 % (Gobbi et al. 2024), and the waste heat is rejected to the coolant circuit. The motor is electrically connected to the inverter model, providing a constant voltage level for the motor. A fixed efficiency of 97 % (Sorokina et al. 2021) is assumed, and the waste heat is

rejected to the coolant. The inverter is connected to the battery system that includes a high-voltage network. Furthermore, a low-voltage network provides energy for additional consumers such as ignition and infotainment. The high-voltage network is connected to an external charging station. Activation of the charging station can be requested by the drive cycle or can be time-based. A battery management controller sets the charge power based on charge maps. The charge maps use the actual battery temperature and state of charge to calculate the suitable charging power. While discharging, the battery management ensures de-rating for battery temperatures that are too high or too low as well as for voltages that are too low voltages.

2.3 Battery Model

The battery system is one of the key components of the vehicle model. Therefore, it is modeled in detail. Parts of the model were described before by Hellmuth, Steeb, Tegethoff, et al. (2022), Steeb et al. (2019), and Hellmuth, Steeb, Pollak, et al. (2023). We model a battery cell including copper and aluminum current arresters, a thermal interface material (gapfiller) and a simplified cooling plate model. The cooling plate is designed as bottom mounted cooling with round channel coils using a water-glycol coolant. Further discussion on cooling plate design can be found in Epp et al. (2023). One representative battery cell is modeled in details and the voltage, current, and heat flows are scaled up to the system level. The battery system is designed for a voltage supply of 800 V. The battery capacity for the baseline scenario is 473.6 kWh.

A pouch cell is chosen because solid-state batteries require high external pressure and only pouch cells can cope with this requirement (Yin et al. 2024). The battery cell is modeled in a 3D-discretization in Modelica. Figure 3 shows the modeling of the battery cell including the conductors, gapfiller, and cooling plate. In this sketch, the battery cell is discretized in length (x), thickness (y) and height (z). That approach is suited for vehicle simulation as the thermal interactions of the battery with other components are at the top (current arresters) and bottom (cooling plate). Automotive battery cells are usually relatively thin. The battery model comprises a network of 9 battery bundles. Each bundle represents a part of the battery cell including a part of the volume, mass, and thermal capacity along with the number of bundles (Veth et al. 2014). A thermal network is calculated in each bundle. The thermal network is built up from thermal resistors and a thermal capacity. The thermal capacity is implemented as a point mass in the center of each discretization element and is parameterized using the mass and heat capacity of the battery cell. Each resistor uses half of the element's size in a geometrical direction and the thermal conductivity. The thermal properties are assumed for the cell as a homogeneous block with anisotropic thermal conductivity (Wendland 2021).

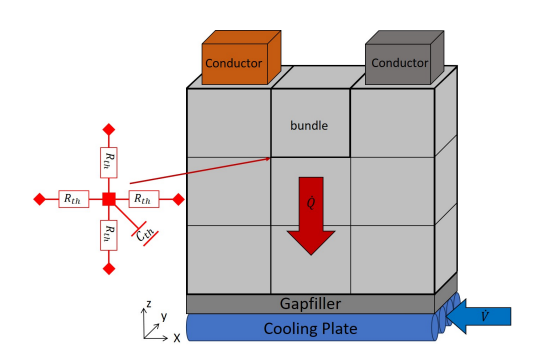


Figure 3. Illustration of a discretized battery cell with one bundle highlighted. Each bundle comprises a thermal network. The system includes conductors, a gapfiller and the cooling plate, adapted from Hellmuth, Steeb, Pollak, et al. (2023).

The battery cell model contains an equivalent circuit model (ECM) as well as a reversible heat model for calculating irreversible heat production (\dot{Q}_{irrev}) and reversible (\dot{Q}_{rev}) heat (Bernardi, Pawlikowski, and Newman 1985) The ECM calculates \dot{Q}_{irrev} based on the internal resistance R_i of the battery cell:

$$\dot{Q}_{irrev} = R_i \cdot I^2 \tag{2}$$

ECM models contain electrical elements such as *Capacitor*, *Ohmic resistances* or *Warburg diffusion*. The models can be parametrized by resistance data of the cell or data obtained from *Electrochemical Impedance Spectroscopy* (EIS) measurements (Westerhoff 2019). For this study, a simple *R1RC* model (see Figure 4) is chosen as sufficient data are provided for that model complexity and accuracy.

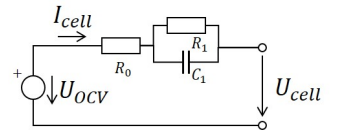


Figure 4. R1RC ECM model adapted from Westerhoff (2019).

The reversible heat model uses the entropy coefficient $\frac{\partial U_{OCV}(T,SoC)}{\partial T}$ to calculate the reversible heat \dot{Q}_{rev} at a certain temperature and a given current:

$$\dot{Q}_{rev} = I \cdot T \cdot \frac{\partial U_{OCV}(T, SoC)}{\partial T}$$
 (3)

From equations 2 and 3, the irreversible and reversible heat dependence on the current I can be analyzed. For calculating the irreversible heat, the current I is squared. The reversible heat depends linearly on the current I. The reversible heat can be released or consumed, depending on the entropy coefficient for different temperatures and different states of charge (SoC). A dependence on the battery state of health (SoH) is not implemented due to a lack of available data yet. A measurement for the load on the battery is the C-Rate, defined as: C-rate $=\frac{I}{Capacity}$

The battery data for this study are obtained from the publication of Yang et al. (2024). They compared the thermal characteristics of a solid-state battery (NMC-S) with one LFP battery and one liquid NMC (NMC-L) battery. Actually, the solid-state battery is a hybrid solid-liquid battery, also called semi-solid (Schmaltz, Hartmann, et al. 2023). In this study, we use the NMC-S and NMC-L battery data for comparison. The NMC-S battery was provided by ProLogium Technology Ltd and the NMC-L is a state-of-the-art battery from CENAT New Energy Ltd. The NMC-S battery uses NMC for the positive electrode and graphite for the negative electrode. The solid electrolyte is made of Li₇La₃Zr₂O₁₂ (LLZO). Some LiPF₆ liquid is added for filling the interface gap, making it a hybrid (Yang et al. 2024). LLZO is a Garnet-type oxide solid electrolyte and one of the most promising options (Schmaltz, Wicke, et al. 2022). Data of both batteries are compared in Table 2:

Table 2. Battery data for the NMC-S and NMC-L, adapted from Yang et al. (2024).

Parameter	NMC-S	NMC-L
Length X (mm)	300	311
Thickness Y (mm)	5.5	7.35
Height $Z(mm)$	100	100
Volume (<i>L</i>)	0.165	0.228
Mass (kg)	0.377	0.520
Nominal Capacity (Ah)	21.3	20
Nominal Voltage (V)	3.6	3.7
Operating Voltage (V)	4.2 - 2.5	4.2 - 2.5
Gravimetric Energy Density	203.4	142.3
$(\frac{Wh}{kg})$		
Volumetric Energy Density	464.7	323.7
$(\frac{Wh}{L})$		
Max Currents	3 <i>C</i>	2 <i>C</i>

The NMC-S battery cell is 27.6 % smaller in volume and 27.5 % lighter in mass and has a slightly higher battery capacity. This results in a much higher gravimetric and volumetric energy density. The operating voltages are similar. The NMC-S battery could be charged or discharged with 3 *C*, while the NMC-L is limited to 2 *C*.

In the first step, both battery systems are designed for the same energy capacity. A 800 V battery system needs approximately 200 battery cells to be connected in series. For the lower nominal voltage, the NMC-S battery is equipped with 205 battery cells in series. To reach the same energy capacity, the NMC-S system is equipped with 30 cells in parallel, the NMC-L with 32. This results in a system capacity of approximately 470 kWh. The battery system data are compared in Table 3.

2.4 Thermal Management

The thermal management in the coach is based on a reversible heat pump using the natural refrigerant R744 and

Table 3. Battery system comparison for NMC-S and NMC-L.

Parameter	NMC-S	NMC-L
Battery Cells (–)	6150	6400
System Volume (<i>L</i>)	1010	1460
System Mass (kg)	2318	3328
Energy Capacity (kWh)	471	473
Nominal Voltage (V)	738	740

additional cooling circuits using a water-glycol coolant. The reversible heat pump provides cooling, heating, and dehumidifying for the cabin, as well as a connection to the cooling circuit. The cooling circuit provides cooling for the battery, motor, and inverter. Waste-heat recovery could also be enabled.

A detailed cabin model (TLK-Thermo GmbH 2024b; Kaiser 2019) was implemented, which models the transient behavior. The interior model is divided into three discretization sections that enable consideration of specific effects, such as the solar radiation on the windshield, and the extraction of recirculated air and supply air from the roof-mounted system in the middle zone. Components, such as the windows and roof, are modeled with their thermal properties. The heat exchangers required for cabin air conditioning are placed in the *Roofbox* and the *Frontbox* (Kaiser 2019).

The reversible R744 heat pump is modeled with the liquid, refrigerant, and gas components provided by the *TIL suite* (TLK-Thermo GmbH 2024b) that enable numerically efficient modeling of thermodynamic systems (Schulze 2013). Components, such as the heat exchangers, are modeled in detail. The main cooling and heating capacity is provided for the cabin. The implemented heat pump uses a four-way-valve for reversing the refrigerant cycle and the secondary loop coolant circuit is used for cooling and heating of the *Frontbox* (Weinreuter and Yildirim 2024). Similar thermal management systems are discussed in previous publications (Hellmuth, Steeb, Pollak, et al. 2023; Hellmuth, Pollak, Schulte, et al. 2024).

The battery cooling circuit operates at temperature levels from $20-40\,^{\circ}\text{C}$ for liquid batteries and up to $40-60\,^{\circ}\text{C}$ for solid-state batteries. For the solid-state battery a de-rating of power is begins above $70\,^{\circ}\text{C}$. A connection to the low temperature cooling circuit allows mixing cold coolant into the circuit, dissipating the battery heat and keeping the temperature level. Different control concepts for various operating strategies and ambient conditions are implemented with a set of *PI-Controllers*. The cabin cooling is prioritized during driving. For fast-charging, the operation strategy shifts to a battery cooling priority. Further optimizations are performed, such as using a dynamic *Gascooler* pressure correlation adapted from Kauf (1999) for controlling the system high pressure.

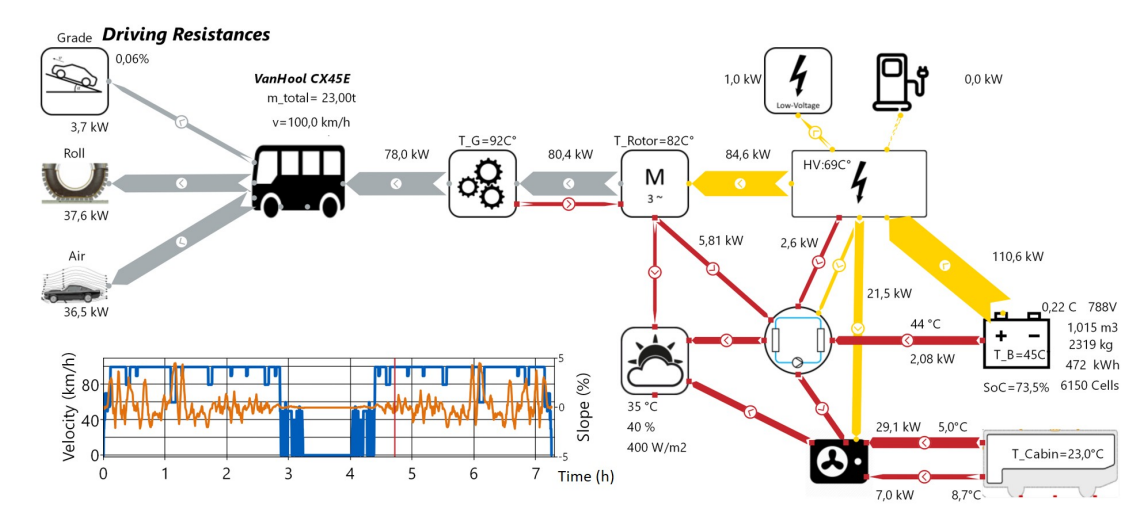


Figure 5. Analysis of energy flows for the NMC-S battery system in the context of the full vehicle, Drive cycle time is indicated by the vertical red line, adapted from Hellmuth, Steeb, Pollak, et al. (2023).

3 Comparison of Battery Systems: Solid-State and Liquid

The solid-state and liquid battery systems are compared in the context of the described long-distance route (see Figure 2). First, the energy flow in the full-vehicle context is evaluated. Next, the battery systems are compared for the same energy capacity. Finally, the systems are compared for the same battery system volume, but different energy capacities.

3.1 Analysis of Energy Flow in the Vehicle

The analysis of energy flows is performed with the software DaVE (TLK-Thermo GmbH 2024a). Analyzing energy flows in the full-vehicle context helps to understand cross-couplings in the complex system. The energy flows are depicted in Figure 5. The NMC-S system is taken. At the driving cycle time of the snapshot, the coach drives up a slight incline at a velocity of $100 \ km/h$. This results in a relatively equal distribution of the required power into grade, roll and air resistance. The efficiencies of the mechanical and electrical components can be obtained from the higher electrical energy flow values towards the battery. $110.6 \ kW$ electrical power is provided. The battery has a SoC of $73.5 \ \%$ and the C-rate is 0.22. The battery system voltage is at $788 \ V$.

The snapshot was taken for the driving scenario at an ambient temperature of 35 °C, an ambient humidity of 40 % and a solar intensity of 400 $\frac{W}{m^2}$. Under these conditions, thermal management adds about 25 % to the electrical energy consumption required for the motor. Additionally, 1 kW of electrical power is needed in the low-voltage network for entertainment, lights, and further demands.

The solid-state battery is conditioned to 45 °C and at

point in the drive cycle very little cooling is necessary. Therefore, only 2.1~kW of heat is transferred to the thermal management. The cabin is conditioned to $23~^{\circ}\text{C}$ and therefore, fresh air is provided at a temperature of $5~^{\circ}\text{C}$ for the main cabin and $8.7~^{\circ}\text{C}$ for the *Frontbox*. A total of 36.1~kW of cooling power is required for cabin cooling.

3.2 Comparison for same Battery System Energy Capacity

As described above, both battery systems are designed for the same energy capacity. They are compared for the Karlsruhe - Munich - Karlsruhe (Figure 2) long-distance drive cycle. The comparison of both battery systems in terms of battery temperature and SoC is displayed in Figure 6. The NMC-L discharges a little bit faster because it needs slightly more energy for battery cooling while the NMC-S battery is not cooled while driving. The other reason for the higher energy consumption is the higher weight of the NMC-L bus. Also, the NMC-L battery system weighs 1000 kg more, resulting in higher grade and roll resistances while driving.

The battery temperature setpoint for the NMC-S is set to 45 °C. In the first driving section, prior to fast-charging which occurs just after the of hour three of the drive cycle, the battery temperature rises from an initial value of 35 °C up to close 40 °C and stays at that temperature level. Therefore, it is not cooled. The NMC-L is cooled to 30 °C to reduce battery degradation. During fast-charging, NMC-S warms up sharply to 59 °C, due mainly to the high internal resistances of the cell and high currents supplied in the fast-charging process. The NMC-L only warms up to 34 °C. This is attributable to the significantly lower internal resistance.

Figure 7 shows the heat produced by the battery

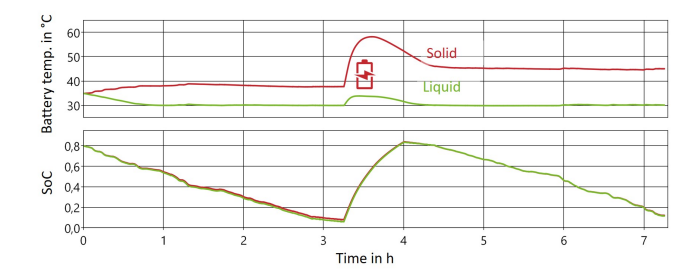


Figure 6. Comparison of the solid-state (NMC-S) and liquid (NMC-L) battery systems along the drive cycle: Battery temperature and SoC.

systems. The heat produced is generally relatively small in normal driving conditions due to the low C-rates. When comparing battery capacity and maximum motor power, the C-rate is limited to a value of $0.76\,C$ while driving; $0.1-0.3\,C$ is typical. This results in relatively low irreversible heat as the currents are squared in calculating it. During fast-charging, the C-rate reaches a maximum close to a value of $2\,C$ ($1\,MW$ charging). Therefore, the irreversible heat production peaks at $82\,kW$ for the NMC-S and at $36\,kW$ for the NMC-L. The higher irreversible heat production results from the internal resistances that are higher by the factor 2.3, even at the elevated temperature of the NMC-S.

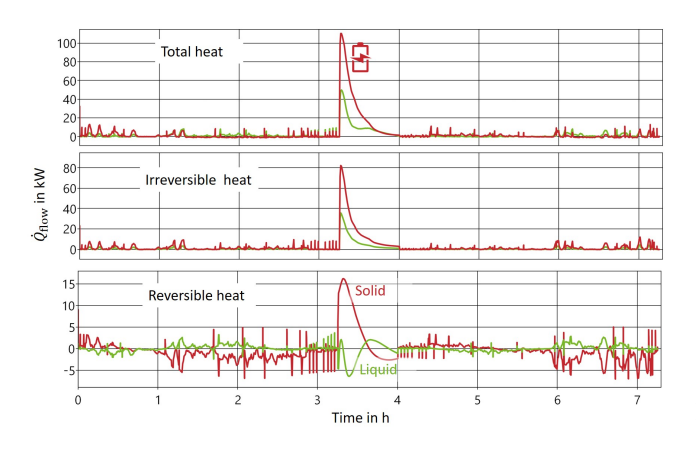


Figure 7. Comparison of battery systems along the drive cycle: Total battery heat, irreversible heat and reversible heat.

The reversible heat can be released or consumed. For the NMC-S, it is negative most of the time while it is discharging (SoC < 0.6), with some positive peaks for recuperation. If the reversible heat is negative, it reduces the total battery heat. The reversible heat dominates for low C-rates; therefore, the battery temperature does not increase for most of the time during normal driving for the NMC-S. Then, at the beginning of charging, it is positive and increases the total heat. For the NMC-L battery, the reversible heat turns to negative values while charging and reduces the produced heat.

3.3 Comparison for same Battery System Volume

In the previous section, it was shown that the solid-state battery heats up to significantly higher temperatures due to higher internal resistances. Because of the higher volumetric and gravimetric energy density, the NMC-S system is smaller and lighter. Assuming a given space for the battery system, sizing the battery systems for the same volume is a logical next step in their comparison. The adjusted parameters for the two battery systems are listed in Table 4:

Table 4. Battery system comparison for NMC- S and NMC- L. Batteries are sized for the same system volume.

Parameter	NMC-S	NMC-L
Battery Cells (–)	8815	6400
System Volume (<i>L</i>)	1450	1460
System Mass (kg)	3323	3328
Energy Capacity (kWh)	676	473
Nominal Voltage (V)	738	740

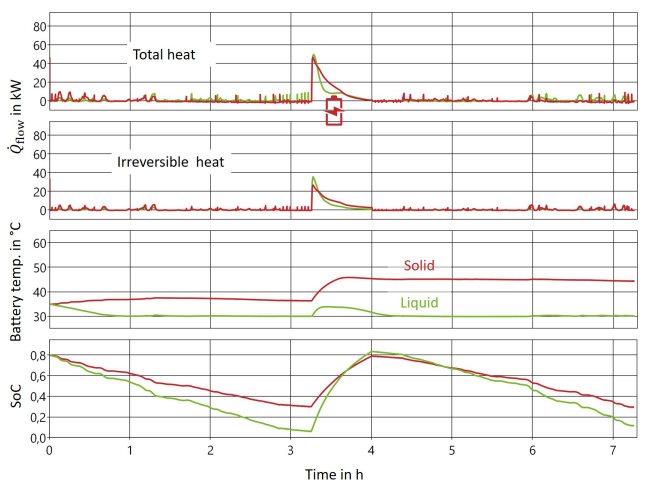


Figure 8. Comparison of batteries at the same system volume along the drive cycle: Total battery heat, irreversible heat, battery temperature and SoC.

In this configuration, both battery systems have approximately the same volume and weight. The NMC-S system has a 43 % higher energy capacity. A comparison of heat flow, battery temperature and SoC for the drive cycle is depicted in Figure 8. The higher energy capacity of the NMC-S leads to much lower C-rates during driving and charging. For this reason, the heat produced by the NMC-S battery is in the same range as that of the NMC-L. The lower C-rates due to the higher capacity compensate for higher internal resistances regarding heat production. Actually, not much cooling is necessary for the large NMC-S. It does not reach the upper setpoint temperature of 45 °C driving to Munich, but slowly heats

up to it during fast-charging.

In the previous comparison, the solid-state battery system's full potential for fast charging is not utilized. In the fast charging it is only charged with a C-rate of 1 C, while up to 3 C would be possible. Also, the battery reaches the charging stop at an SoC of 0.3, so charging is not needed. For a simple scenario adjustment, the bus with the NMC-S battery starts at a SoC of only 0.6 and the charging break is reduced to 30 minutes. Therefore, the charging station is modified to allow up to 2 MW of charging power, which is likely to be possible at large charging stations in the future (Makoschitz 2022).

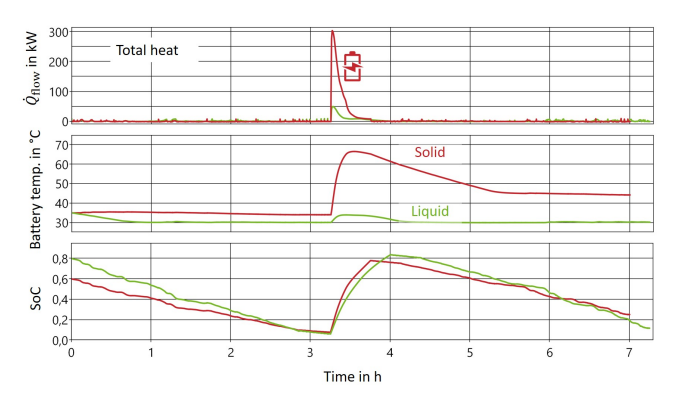


Figure 9. Comparison of batteries at the same system volume along the drive cycle with faster charging for NMC-S battery: Total battery heat, battery temperature and SoC.

An evaluation of the adjusted scenario is depicted in Figure 9. The bus with the NMC-S battery charges in just 30 minutes with a C-rate of up to 2.8 C to an SoC of 80 %. The bus reaches the final destination in Karlsruhe 15 minutes faster with a SoC of 0.25 remaining. During the first driving section from Karlsruhe to Munich, the NMC-S battery does not rise in temperature, due to the low currents and correspondingly low irreversible heat flows. The reversible heat is mostly negative at the low SoCs, so the battery consumes heat. Both effects roughly cancel each other out resulting in a constant battery temperature at the initial 35 °C. The high currents during fast charging result in a heat flow of up to 300 kW for a short time. The battery temperature rises rapidly during charging to 67 °C, this is still below the set de-rating temperature of 70 °C for the solid-state battery. After charging, the battery is slowly cooled down to the operating temperature of 45 °C.

The slow cool-down is caused by the current thermal management battery cooling capacities. More data on degradation of solid-state batteries would be needed for evaluating if such high temperatures for a longer time accelerate battery degradation significantly. The thermal management could be re-designed for enabling higher battery cooling capacities. Different operating strategies optimizing battery degradation and thermal management en-

ergy consumption could be tested by system simulation as has been done before for battery-electric heavy-duty trucks (Hellmuth, Steeb, Pollak, et al. 2023).

4 Conclusions

In our study, we demonstrated that a physics-based full-vehicle Modelica model of a battery-electric coach paired with real-world drive scenarios can be used efficiently to compare different types and configurations of battery systems. We implemented battery data from a recent study (Yang et al. 2024) for a liquid NMC battery and a (semi-) solid-state battery into the vehicle model and designed different battery systems. Furthermore, we modeled a state-of-the-art thermal management system using the natural refrigerant R744.

Our results show that in general the higher internal resistances of solid-state batteries lead to higher heat production in the battery system. This is especially the case for fast-charging with high C-rates. The higher operation temperatures of solid-state batteries partially compensate for that. For normal driving of a coach, C-rates are typically very low, resulting in small heat loads. Additionally, the reversible heat plays a role, providing cooling at some operation points. In our first battery system design, both systems are sized for the same energy capacity. The NMS-S produces more heat, but saves weight and only heats up significantly during fast-charging. The maximum temperature during charging of 59 °C is still within the operation limits.

The second battery system design uses the same size or battery volume. Therefore, the solid-state battery has a 43 % higher energy capacity and respectively, lower C-rates during operation. Therefore, the heat production is in a similar range as for the liquid battery.

Future research should evaluate use cases for cold ambient temperatures and discuss battery pre-heating strategies and cold-start performances. Furthermore, battery waste-heat utilization for cabin heating should be explored. Battery degradation, cabin comfort goals as well as thermal management energy consumption should be considered. For this, different thermal management system topologies and operation strategies will need to be evaluated.

Acknowledgments

Our work was funded by the European Regional Development Fund (ERDF) in the EUROPA FÜR NIEDERSACH-SEN funding as part of the TOFEBAS research project. The authors would like to thank the student assistants Jonte Tiedemann and Luca-Leon Lohnert for their help in preparing the data and models.

References

- Bernardi, D., E. Pawlikowski, and J. Newman (1985). "A General Energy Balance for Battery Systems". In: *Journal of The Electrochemical Society* 132.1, pp. 5–12. DOI: 10.1149/1.2113792.
- Epp, Alexander et al. (2023). "Simulative Investigation of Optimal Multiparameterized Cooling Plate Topologies for Different Battery System Configurations". In: *Energy Technology* 11.9. ISSN: 2194-4288. DOI: 10.1002/ente.202300405.
- Gobbi, Massimiliano et al. (2024). "Traction motors for electric vehicles: Maximization of mechanical efficiency A review". In: *Applied Energy* 357, p. 122496. DOI: 10.1016/j.apenergy. 2023.122496.
- Hebeler, Georg Maximilian (2024). "Modellbasierte Potenzialanalyse von Planetengetrieben zur Integration eines Rankine-Prozesses in einen Reisebus". PhD thesis. Technische Universität Braunschweig. DOI: 10 . 24355 / DBBS . 084 -202412101034-0.
- Heinke, Steffen et al. (2019). "High-Temperature Refrigeration System for Cooling of Automotive PEM Fuel Cells". In: 2nd Conference on High Temperature Heat Pumps, Copenhagen, Denmark, September 2019. URL: https://orbit.dtu.dk/en/publications/book-of-presentations-of-the-2nd-symposium-on-high-temperature-he.
- Hellmuth, Jan Friedrich, Markus Pollak, Timo Heinke, et al. (2023). Wärmepumpe für Nutzfahrzeuge mit Feststoffbatterien. DKV-Conference 2023, Hannover, AA III.16.
- Hellmuth, Jan Friedrich, Markus Pollak, Andreas Schulte, et al. (2024). "Assessment of natural refrigerants for thermal management in battery-electric long-distance buses". In: 16th IIR Gustav Lorentzen Conference on Natural Refrigerants, College Park, Maryland, USA 2024. DOI: https://dx.doi.org/10.18462/iir.gl2024.1153.
- Hellmuth, Jan Friedrich, Michael Steeb, Markus Pollak, et al. (2023). "Innovative thermal management operathellmuing strategies for battery-electric heavy-duty trucks". In: Proceedings of the ECOS Conference 2023, Las Palmas de Gran Canaria. DOI: 10.24355/DBBS.084-202310260841-0.
- Hellmuth, Jan Friedrich, Michael Steeb, Wilhelm Tegethoff, et al. (2022). "Thermische Simulation im Gesamtfahrzeugkontext". In: *Werkstoffsymposium 2022, Wolfsburg, 17.-18. Mai 2022.*
- Hughes, Ryan and Christopher Vagg (2022). "Assessing the Feasibility of a Cold Start Procedure for Solid State Batteries in Automotive Applications". In: *Batteries* 8.2, p. 13. DOI: 10. 3390/batteries8020013. URL: https://www.mdpi.com/2313-0105/8/2/13.
- Janek, Jürgen and Wolfgang G. Zeier (2023). "Challenges in speeding up solid-state battery development". In: *Nature Energy* 8.3, pp. 230–240. ISSN: 2058-7546. DOI: 10.1038/s41560-023-01208-9. URL: https://www.nature.com/articles/s41560-023-01208-9.
- Kaiser, Christian (2019). "Untersuchungen zur Effizienz- und Leistungssteigerung von Omnibusklimaanlagen". Dissertation. Braunschweig: Technische Universität Braunschweig. DOI: 10.24355/dbbs.084-202005181332-0.
- Kan, Ruyu et al. (2024). "Thermal effects of solid-state batteries at different temperature: Recent advances and perspectives". In: *Energy Storage Materials* 68, p. 103366. DOI: 10.1016/j. ensm.2024.103366.
- Kauf, Friedrich (1999). "Determination of the optimum high pressure for transcritical CO2-refrigeration cycles". In: *In-*

838

- ternational Journal of Thermal Sciences 38.4, pp. 325–330. DOI: 10.1016/S1290-0729(99)80098-2.
- Li, Haibin et al. (2025). "Electro-thermal coupling modeling and heat generation decoupling analysis of semi-solid-state lithium-ion battery". In: *Electrochimica Acta* 512, p. 145455. ISSN: 0013-4686. DOI: 10.1016/j.electacta.2024.145455.
- Ma, Xiaole et al. (2025). "Modelling and verification of the electro-thermal coupling model for solid-state batteries based on equivalent circuit model". In: *Applied Thermal Engineering* 269, p. 126063. DOI: 10.1016/j.applthermaleng.2025. 126063.
- Makoschitz, Markus (2022). "Key aspects to enable multimegawatt fast charging". In: *e & i Elektrotechnik und Informationstechnik* 139.4-5, pp. 435–448. ISSN: 0932-383X. DOI: 10.1007/s00502-022-01037-w.
- Modelica Association (2025). *Modelica A Unified Object-Oriented Language for Systems Modeling: Language Specification: Version 3.6.* URL: https://specification.modelica.org/maint/3.6/MLS.pdf.
- Sanguesa, Julio A. et al. (2021). "A Review on Electric Vehicles: Technologies and Challenges". In: *Smart Cities* 4.1, pp. 372–404. DOI: 10.3390/smartcities4010022.
- Schmaltz, Thomas, Felix Hartmann, et al. (2023). "A Roadmap for Solid–State Batteries". In: *Advanced Energy Materials* 13.43. ISSN: 1614-6832. DOI: 10.1002/aenm.202301886.
- Schmaltz, Thomas, Tim Wicke, et al. (2022). *Solid-State Battery Roadmap* 2035+. DOI: 10.24406/publica-68.
- Schulze, Christian Wilhelm (2013). "A Contribution to Numerically Efficient Modelling of Thermodynamic Systems". Dissertation. TU Braunschweig. DOI: 10.24355/dbbs.084-201409121113-0.
- Sorokina, Nina et al. (2021). "Inverter and Battery Drive Cycle Efficiency Comparisons of Multilevel and Two-Level Traction Inverters for Battery Electric Vehicles". In: 2021 IEEE International Conference on Environment and Electrical Engineering and 2021 IEEE Industrial and Commercial Power Systems Europe (EEEIC / 1&CPS Europe). IEEE, pp. 1–8. ISBN: 978-1-6654-3613-7. DOI: 10.1109/EEEIC/ICPSEurope51590.2021.9584705.
- Steeb, Michael et al. (2019). "Avoiding Thermal Hotspots in Automotive Battery Systems using a Multiscale Full Vehicle Model". In: 16th Symposium on Modeling and Experimental Validation of Electrochemical Energy Technologies, Braunschweig, 12.-13. March 2019.
- Sustainable Bus (2020). *Van Hool electric coach is reality. The first unit of the CX45E shipped to the US*. URL: https://www.sustainable-bus.com/news/van-hool-electric-coach-cx45e-usa/.
- Thomas, Hugh and André Cabrera Serrenho (2024). "Using different transport modes: An opportunity to reduce UK passenger transport emissions?" In: *Transportation Research Part D: Transport and Environment* 126, p. 103989. ISSN: 1361-9209. DOI: 10.1016/j.trd.2023.103989. URL: https://www.sciencedirect.com/science/article/pii/S1361920923003863.
- TLK-Thermo GmbH (2024a). *DaVE*. URL: https://www.tlk-thermo.com/en/software/dave.
- TLK-Thermo GmbH (2024b). *TIL-Suite*. URL: https://www.tlk-thermo.de/en/software/til-suite.
- UK Department for Business Energy & Industrial Strategy (2022). Government conversion factors for company reporting of greenhouse gas emissions. URL: https://www.gov.uk/government/publications/greenhouse-gas-reporting-conversion-factors-2024.

10.3384/ecp218831

- Veth, C. et al. (2014). "Electro-Thermal Model Approach for the Prediction of Internal State Values in Large-Format Lithium Ion Cells and Its Validation". In: *Electrochem. Soc. 161 (14)*, *A1943-A1952*. DOI: https://doi.org/10.1149/2.1201412jes.
- Weinreuter, Tobias and Kemal-Edip Yildirim (2024). *Modulares Thermomanagement in Bussen mit batterieelektrischem Antrieb in Verbindung mit einer R744 Wärmepumpe*. 13. VDI-Fachkonferenz Thermomagement für elektromotorisch angetriebene PKW, 27.11.2024, Aachen.
- Wendland, Robert (2021). "Ein Beitrag zur thermischen Auslegung von Fahrzeug-Batteriesystemen". Dissertation. Technische Universität Braunschweig. DOI: 10.24355/dbbs.084-202106241143-0.
- Westerhoff, Uwe (2019). "Klassifizierung von Lithium-Ionen-Batteriezellen mittels kenngrößenbasierter Methoden". Dissertation. Technische Universität Braunschweig, Verlag Dr. Hut. ISBN: 978-3-8439-4179-2.
- Yang, Rui et al. (2024). "Comparative Study on the Thermal Characteristics of Solid-State Lithium-Ion Batteries". In: *IEEE Transactions on Transportation Electrification* 10.1, pp. 1541–1557. DOI: 10.1109/TTE.2023.3289997.
- Yin, Zhen et al. (2024). "Battery Management System Towards Solid-State Batteries". In: *IEEE CHAIN* 1.4, pp. 319–353. DOI: 10.23919/CHAIN.2024.000011.